2015

Reassessment of the role of aromatic amino acid hydroxylases and the effect of infection by Toxoplasma gondii on host dopamine

Zi T. Wang
Washington University School of Medicine in St. Louis

Steve Harmon
Washington University School of Medicine in St. Louis

Karen L. O'Malley
Washington University School of Medicine in St. Louis

L David Sibley
Washington University School of Medicine in St. Louis

IAI Journals.ASM.org

Reassessment of the Role of Aromatic Amino Acid Hydroxylases and the Effect of Infection by *Toxoplasma gondii* on Host Dopamine

Zi T. Wang,[a] Steve Harmon,[b] Karen L. O'Malley,[b] L. David Sibley[a]

Department of Molecular Microbiology[a] and Department of Anatomy and Neurobiology,[b] School of Medicine, Washington University in St. Louis, St. Louis, Missouri, USA

***Toxoplasma gondii* infection has been described previously to cause infected mice to lose their fear of cat urine. This behavioral manipulation has been proposed to involve alterations of host dopamine pathways due to parasite-encoded aromatic amino acid hydroxylases. Here, we report successful knockout and complementation of the aromatic amino acid hydroxylase *AAH2* gene, with no observable phenotype in parasite growth or differentiation *in vitro* and *in vivo*. Additionally, expression levels of the two aromatic amino acid hydroxylases were negligible both in tachyzoites and in bradyzoites. Finally, we were unable to confirm previously described effects of parasite infection on host dopamine either *in vitro* or *in vivo*, even when *AAH2* was overexpressed using the *BAG1* promoter. Together, these data indicate that AAH enzymes in the parasite do not cause global or regional alterations of dopamine in the host brain, although they may affect this pathway locally. Additionally, our findings suggest alternative roles for the *AHH* enzymes in *T. gondii*, since *AAH1* is essential for growth in nondopaminergic cells.**

The protozoan parasite *Toxoplasma gondii* is an obligate intracellular parasite that is capable of infecting most warm-blooded animals. It is a member of the phylum *Apicomplexa*, which also contains *Plasmodium falciparum*, the causative agent of malaria. *Toxoplasma gondii* is one of the most widely distributed parasites in the world, both in geographic location and in the diversity of its host range (1). Its only definitive hosts are members of the genus *Felis*. Exclusively within enterocytes of the gut, it undergoes a sexual reproductive cycle to form environmentally resistant and infectious oocysts that are shed in cat feces (2). In all other hosts, *Toxoplasma gondii* infection begins as a fast-growing lytic stage called the tachyzoite. Innate and adaptive immune responses restrict the growth of tachyzoites, which can respond by differentiating into bradyzoites, a semidormant stage that exists as quiescent intracellular cysts in brain and muscle tissue. This chronic infection can persist for the lifetime of the host (3). Infections spread among incidental hosts through carnivorism, vertical transmission, and ingestion of *T. gondii* oocysts (4).

Rodents that become infected by *T. gondii* exhibit an unusual behavioral response: they lose their instinctive aversion to the odor of cats and instead become mildly attracted to the scent (5–13). This behavioral manipulation appears specific to the cat (7, 8), and it has been speculated that this facilitates transmission (9). The exact mechanism of this behavioral manipulation is unknown, but parasite stimulation of host dopamine pathways in the brain has been suggested as a cause (14–16). It was observed that infection of mice by *T. gondii* caused a 14% increase in whole-brain dopamine levels upon establishment of chronic infection (17). Additionally, dopamine receptor antagonist drugs used for the treatment of schizophrenia block cat attraction in infected rodents (18, 19). *T. gondii* infection also was described to increase dopamine content and dopamine release in the dopaminergic cell line PC12 *in vitro* (15).

The mechanism by which infection might alter dopamine is unknown, but it has been suggested that parasite metabolism contributes to elevated dopamine levels (20). The *T. gondii* genome contains two genes that encode aromatic amino acid hydroxylases (AAAH), which carry out the rate-limiting step of dopamine synthesis in metazoans by converting tyrosine into the dopamine precursor 3,4 dihydroxyphenylalanine (L-Dopa) (20). The two nearly identical genes *AAH1* and *AAH2* contain putative signal peptides targeting them for secretion, and both appear to be functional tetrahydrobioptern-dependent aromatic amino acid hydroxylases *in vitro* (20). *AAH1* was reported to be constitutively expressed, while the expression of *AAH2* was reported to increase in the dormant bradyzoite stage (20). Because of this pattern, *AAH2* was suggested to be the prime candidate effector of the parasite's manipulation of host dopamine (20).

We sought to test the hypothesis that the aromatic amino acid hydroxylases *AAH1* and/or *AAH2* were responsible for causing alterations in dopamine metabolism in the host. We successfully knocked out and complemented the *AAH2* gene but, unexpectedly, could not observe a parasite effect on host dopamine levels either *in vitro* with PC12 cells or *in vivo* with mouse infection. Further, we observed that expression of both *AAH1* and *AAH2* was negligible in tachyzoites, and while they both showed increased expression in bradyzoite stages, the relative expression level still was very low. Collectively, our findings indicate that AAH enzymes in *T. gondii* do not cause global alterations of host dopamine; rather, they may participate in alternative pathways.

Received 11 August 2014 **Returned for modification** 19 September 2014
Accepted 22 December 2014

Accepted manuscript posted online 29 December 2014

Citation Wang ZT, Harmon S, O'Malley KL, Sibley LD. 2015. Reassessment of the role of aromatic amino acid hydroxylases and the effect of infection by *Toxoplasma gondii* on host dopamine. Infect Immun 83:1039–1047. doi:10.1128/IAI.02465-14.

Editor: J. H. Adams

Address correspondence to L. David Sibley, sibley@wustl.edu.

Supplemental material for this article may be found at http://dx.doi.org/10.1128/IAI.02465-14.

doi:10.1128/IAI.02465-14

MATERIALS AND METHODS

Parasite strains. Parasites were propagated by serial passage in human foreskin fibroblast (HFF) cells grown in Dulbecco's modified Eagle medium (DMEM; Life Technologies, Carlsbad, CA) containing 10% fetal bovine serum (FBS) (HyClone, Logan, UT), 10 mM HEPES, pH 7.4, 1 mM glutamine, 10 μg/ml gentamicin, under 5% CO_2 at 37°C (D10 medium). The PruΔ*ku80*Δ*hxg* strain (type II) was obtained from John Boothroyd (21). The ME49 strain (type II) (ATCC 50611; American Type Culture Collection, Manassas, VA) originally was isolated from sheep diaphragm (22). The C56 strain (type III) originally was isolated from a chicken (23). PC12 cells (ATCC CRL-1721) were obtained from the ATCC and cultured in RPMI 1640 medium (ATCC) supplemented with 10% heat-inactivated horse serum (Life Technologies) and 5% FBS (PC12 medium). SH-SY5Y cells (ATCC CRL-2266), confirmed to be mycoplasma negative, also were obtained from the ATCC and cultured in a 1:1 mixture of ATCC Eagle's minimum essential medium and F12 medium supplemented with 10% FBS (SH-SY5Y medium).

Generation of deletion plasmids. To generate a deletion plasmid targeting the AAH2 locus, regions 1.1 kb upstream and 1.8 kb downstream from the AAH2 locus were PCR amplified from ME49 genomic DNA using primers listed in Data Set S1 in the supplemental material and were cloned into pDONR-p4p1r and pDONR-p2rp3 vectors, respectively (Invitrogen). Using the Gateway 3-fragment system, the upstream and downstream flanks and a central HXGPRT expression cassette cloned into pDONR-p1p2 were assembled into pDEST-R4R3 to create the plasmid pHXG-Δ*aah2*.

Generation of AAH2 cleanup and complementation plasmids. To generate a plasmid to remove HXGPRT from the AAH2 locus, the 1.1-kb upstream and 1.8-kb downstream regions were PCR amplified from ME49 genomic DNA with primers that added a 20-bp overlap. The pieces then were fused by PCR and cloned into pDONR-p4p1r to create plasmid pΔaah2. To complement AAH2, the cDNA of AAH2 was amplified from a PruΔ*ku80*Δ*hxg* cDNA sample, and the 1.1-kb upstream region with an ~20-bp overlap into the 5′ end of the AAH2 coding sequence and the 1.8-kb downstream region with an ~20-bp overlap into the 3′ end of the AAH2 coding sequence were amplified from PruΔ*ku80*Δ*hxg* genomic DNA (gDNA). The three pieces were fused by PCR and cloned into pDONR-p4p1r to create the plasmid p::AAH2.

Generation of AAH1/AAH2 tagging and AAH2 BAG1 overexpression plasmids. To generate plasmids to tag AAH1/AAH2, primers were designed to amplify 1.5 kb of the 3′ end of the gene with the addition of a Ty epitope (24) before the stop codon and to amplify 600 bp of the 3′ UTR of the gene with the same addition. These two pieces were fused by PCR and cloned into pDONR-p4p1r. A 1.5-kb region 1.5 kb downstream from the stop codon was cloned into pDONR-p2rp3, and the pieces were combined with HXGPRT-pDONR-p1p2 to create the tagging plasmids pAAH1::Ty and pAAH2Ty. To generate a plasmid to drive AAH2 with the BAG1 promoter, primers were designed to amplify 900 bp of the 5′ UTR of BAG1 with an ~20-bp overlap into the AAH2 coding sequence, the cDNA of AAH2 with a Ty epitope insertion, and 1.5 kb of the AAH2 3′ UTR with an ~20-bp overlap into the Ty tag and AAH2 coding sequence. These three fragments were fused with end-overlap PCR and cloned into p2rp3. This fusion was combined with a 900-bp region upstream of AAH2 in pDONR-p4p1r and the HXGPRT cassette in pDONR-p1p2 into pDEST-R4R3 to create the plasmid pBAG1::AAH2Ty.

Generation of parasite transgenic lines. To generate transgenic lines, PruΔ*ku80*Δ*hxg* parasites were transfected with DNA PCR amplified from the critical regions of recombinant plasmids. Following the transfection of amplified DNA (5 to 15 μg), parasites were allowed to recover on HFF monolayers for 24 h before positive selection for the HXGPRT cassette with 25 μg/ml mycophenolic acid (Sigma-Aldrich) supplemented with 50 μg/ml xanthine (Sigma-Aldrich) (25) or negative selection against HXGPRT with 340 μg/ml 6-thioxanthine (26). Resistant parasites were cloned by limiting dilution into 96-well plates containing HFF monolayers and screened by PCR.

***In vitro* differentiation.** Parasites were differentiated using 48 h of treatment with sodium bicarbonate-free RPMI 1640 medium containing 1% FBS and 50 mM HEPES, pH 8.1, at 37°C without CO_2 (27). Parasites in PC12 cells were differentiated using 48 h of treatment with PC12 medium supplemented with 50 mM HEPES, pH 8.1. Parasites in SH-SY5Y cells were differentiated using 48 h of treatment with SH-SY5Y medium supplemented with 50 mM HEPES, pH 8.1.

Infection of mice. Parasites were harvested by syringe lysis of infected HFF cultures at 24 h postinfection using a 22-gauge needle. They then were purified by passage through a 3.0-μm polycarbonate filter (GE Water and Process Technologies, Beaumont, TX), counted by a hemocytometer, and diluted in fresh D10 medium. Eight-week-old female CD1 mice (Charles River Laboratories, Wilmington, MA) were injected intraperitoneally (i.p.) in a volume of 200 μl containing 10^3, 2×10^2, or 10^4 parasites and monitored daily. One month postinfection, mice were euthanized by CO_2 asphyxiation followed by cervical dislocation serially across treatment groups to maximize consistency, and brains were removed for analysis. Animal studies were approved by the Institutional Animal Studies Committee (School of Medicine, Washington University in St. Louis).

Plaque assay. Parasites were syringe lysed from infected HFF monolayers, purified with a 3.0 μm polycarbonate filter, and counted by hemocytometer. Parasites were serially diluted, and 10^3 parasites (100 μl) were seeded onto confluent HFF monolayers in 6-well plates and grown for 11 days at 37°C, 5% CO_2. HFFs were fixed with 70% ethanol for 10 min and then incubated with 0.5% crystal violet in distilled H_2O for 10 min, washed, and scanned with an EPSON Perfection V500 photo scanner.

Immunofluorescence microscopy. Infected monolayers cultured on glass coverslips were fixed and permeabilized with 4% formaldehyde containing 0.5% Triton X-100 for 15 min. Slips were stained with primary antibody that reacts to the Ty tag (24) and fluorescein isothiocyanate (FITC)-conjugated *Dolichos biflorus* lectin (DBL) (Sigma, St. Louis, MO) diluted at 1:1,000 in phosphate-buffered saline (PBS)–5% FBS containing 5% NGS (normal goat serum; Sigma). Primary antibodies were visualized using goat anti-mouse or goat anti-rabbit IgG conjugated to Alexa-594 (Invitrogen Molecular Probes, Carlsbad, CA). Slides were analyzed with a Zeiss AxioSkop wide-field epifluorescence microscope equipped with an AxioCam charge-coupled-device (CCD) camera, and images were captured using AxioVision v3.1 (Carl Zeiss Inc., Thornwood, NY). Using Photoshop CS3 (Adobe, San Jose, CA), images were cropped, color levels were adjusted, and then images were assembled.

qPCR. Tachyzoite and bradyzoite parasites were harvested into calcium-free PBS by syringe lysis of infected HFF cultures and filtration with a 3.0 μm polycarbonate filter. RNA was harvested using a Qiagen RNeasy kit (Qiagen, Valencia, CA). cDNAs were prepared from total RNA (1.0 μg) using 50 μM oligo(dT) (20) and Superscript III reverse transcriptase (RT; Invitrogen) according to the manufacturer's protocols. PCR primers for reference and stage-specific genes were described previously (27), and primers for *AAH1* and *AAH2* were designed using Primer Express software, version 1.0 (Applied Biosystems, Forster City, CA, USA). Real-time quantitative PCR (qPCR) was performed using a SmartCycler (Cepheid, Sunnyvale, CA) in a reaction volume of 25 μl containing SYBR Advantage qPCR premix (Invitrogen), 400 nM each primer, and 1 μl of cDNA. The reaction conditions were 50°C for 2 min, 95°C for 10 min, and then 45 cycles of 95°C for 15 s and 62°C for 30 s. Data analysis was conducted using SmartCycler (Cepheid) software. Relative gene expression levels were calculated as fold change using the threshold cycle (C_T) formula $2^{-\Delta\Delta CT}$, where $\Delta C_T = C_T$ (actin) $- C_T$ (target gene) and $\Delta\Delta C_T = \Delta C_T$ (tachyzoite-stage RNAs) $- \Delta C_T$ (bradyzoite-stage RNAs) (28). The housekeeping gene encoding actin (ACT1) was used as a reference control.

Western blotting. Western blots were done as previously described (29), with the following antibodies: rabbit αGRA2 and mouse monoclonal antibody (MAb) BB2. Primary antibodies were detected with fluorescently conjugated IRDye secondary antibodies (LI-COR, Lincoln, NE) and visualized on an Odyssey infrared imaging system (LI-COR).

ELISA. High-binding enzyme-linked immunosorbent assay (ELISA) plates (Corning, Corning, NY) seeded with parasite antigen (sonicated RH strain lysate in PBS at 10^5 parasites per well) were incubated with serum from chronically infected mice (collected 1 month postinfection) diluted 1:1,000 in PBS-Tween containing 0.1% bovine serum albumin (BSA) for 1 h at room temperature. Antibodies were detected with a 1:5,000 dilution of horseradish peroxidase (HRP)-conjugated goat anti-mouse IgG (Jackson Laboratories, Sacramento, CA) for 1 h at room temperature. HRP activity was captured using BD OptEIA substrate reagent A and substrate reagent B (BD Biosciences, Franklin Lakes, NJ). Absorbance at 450 nm was read using an EL-800 universal microplate reader (Bio-Tek Instruments Inc., Winooski, VT).

Cyst count. Chronically infected animals were euthanized and the brains removed. Brains were homogenized and stained with DBL as previously described (27). Dilutions of stained homogenates were examined using a Zeiss wide-field epifluorescence microscope. Three separate aliquots were counted per brain sample, and total brain cyst load was determined based on the total volume of the brain homogenate (0.6 to 1.0 ml) and the average count per volume (15 to 20 μl).

***In vitro* sample preparation.** Six-well plates were seeded with 300 μl of a 0.01% solution of type IV collagen (Sigma) in 0.1 M glacial acetic acid. After three 1-ml PBS washes to remove residual acetic acid, PC12 cells were seeded at 10^6 cells each into each well and allowed to adhere for 24 h. Filtered parasites were seeded onto PC12s at a multiplicity of infection (MOI) of 1 (one parasite per PC12 cell) and allowed to invade for 4 h. Cells were washed three times with PBS to remove noninvaded parasites and then returned to standard or differentiation culture conditions for 48 h. SH-SY5Y cells were seeded onto 6-well plates at 1×10^6 cells per well. PC12 or SH-SY5Y cells were dislodged from the plate using mechanical pressure from a pipette, counted by hemocytometer, pelleted at 5,000 RCF (relative centrifugal force), and resuspended into 500 μl ice-cold 0.1 N perchloric acid and 0.4 M sodium metabisulfite in distilled H_2O (PCA buffer). Cells were homogenized on ice with a Branson sonifier cell disruptor 185 (three 5-s pulses, power of 3/10) (Danbury, CT) and centrifuged at 14,000 RCF for 15 min at 4°C. The supernatant was filtered through a 0.22-μm filter and diluted into MD-TM buffer (75 mM NaH_2PO_4-H_2O, 1.7 mM octane sulfonic acid, 100 μl/liter triethylamine, 25 μM EDTA, 10% acetonitrile, pH 3.0; ESA, Bedford, MA) for analysis with high-performance liquid chromatography (HPLC).

***In vivo* sample preparation.** Chronically infected mice were euthanized. The brain was removed and cut sagitally along the midline. Half of each brain was weighed, transferred to 500 μl ice-cold PCA buffer, and homogenized by a hand homogenizer, followed by sonication on ice with a Branson sonifier cell disruptor 185 (three 10-s pulses, power of 3/10). Homogenates were spun at 14,000 RCF for 15 min, and the supernatant was collected and filtered through a 0.22-μm filter. Supernatants were diluted into MD-TM buffer for HPLC analysis.

HPLC. HPLC analysis was performed, as described in reference 30, using a Coulochem electrochemical detector (ESA, Bedford, MA) with an ESA MD 150- by 3.2-mm column. The mobile phase consisted of ESA MD-TM buffer. HPLC detection of samples was calibrated using standard samples of dopamine (DA), dopachrome (Dopac), and homovanillic acid (HVA) at 0.1, 0.5, or 1.0 ng/100 μl. The retention times of each catecholamine was determined. The total area under the HPLC trace for five replicate runs of each catecholamine was measured to create the reference curve for subsequent quantitative analysis of catecholamine amounts (see Fig. S1 in the supplemental material).

Statistical testing. qPCR data were analyzed by two-way analysis of variance (ANOVA) with Tukey's multiple-comparison test. *In vitro* HPLC data were analyzed by one-way ANOVA. Cyst count data and *in vivo* mouse dopamine data were analyzed by the Kruskal-Wallis nonparametric test and Dunn's multiple-comparison test. Cyst count versus dopamine data were analyzed by linear regression. Statistical analysis was done in Prism 6 for Mac OSX (GraphPad Software, La Jolla, CA).

RESULTS

Deletion of *AAH2* in the type II PruΔ*ku80*Δ*hxg* background. Previous work has described two highly similar *AAH* genes in *T. gondii* (20). During the course of this work, assembly 9 of the *T. gondii* ME49 genome was released (ToxoDB.org). In this version, only one of the *AAH* genes is found in the chromosome (i.e., *AAH2*), while the other one is on an unassembled contig (i.e., *AAH1* on contig TgME49_asmbl.1705). Because this differs from the genomic organization of the genes in assembly 8 (where they were found in tandem on chromosome V), we PCR mapped and sequenced the regions flanking *AAH1* and *AAH2* from the Pru strain. Our findings were consistent with the arrangement of the previous ME49 genome assembly 8 (see Fig. S2 in the supplemental material).

To examine the role of *AAH2*, a double homologous recombination strategy was employed to target the gene for deletion (Fig. 1A). We transfected knockout constructs into the background strain PruΔ*ku80*Δ*hxg* (21) and selected for positive transfectants using HXG selection (25). The gene was successfully knocked out, creating the knockout strain PruΔ*ku80*Δ*hxg*Δ*aah2*, as shown by the absence of an expected 4.8-kb band encompassing the *AAH2* gene (Fig. 1B). The knockout line then was complemented with a cDNA copy of the *AAH2* gene driven by its endogenous 5′ and 3′ UTRs, creating the complement strain PruΔ*ku80*Δ*hxg*Δ*aah2*::*AAH2*. The complement was confirmed by PCR, showing the presence of a shorter 1.6-kb band consistent with the cDNA of *AAH2* (Fig. 1B). Despite repeated attempts (more than 3) to delete *AAH1* using a similar strategy, we were unable to obtain knockouts of this gene (data not shown), suggesting it is essential.

The parasite *AAH2* is not essential for growth, differentiation, host infection, or oral transmission. To test for overall growth, we compared the ability of knockout and wild-type parasites to form plaques on HFF monolayers. A plaque assay showed no significant defect in growth rate in the knockout (Fig. 1C; also see Fig. S3 in the supplemental material). We next tested the ability of the parasite to convert from the lytic tachyzoite stage to the dormant bradyzoite stage *in vitro* under stress induced by high pH (8.1), a well-established model for *in vitro* differentiation (31). Bradyzoite differentiation under high pH was normal, as measured by FITC-conjugated *Dolichos biflorus* lectin specific to *N*-acetyl galactosamine that is found in the bradyzoite cyst wall (32) (Fig. 2; also see Fig. S4 in the supplemental material).

We next used quantitative real-time PCR to test for abnormalities in bradyzoite induction at the transcriptional level. We examined the change in transcription of the tachyzoite-specific genes *SAG1* and *SAG2A*, bradyzoite-specific genes *BAG1* and *LDH2* (27), as well as our genes of interest, *AAH1* and *AAH2*. As expected, no significant differences in expression levels were seen with either the tachyzoite or the bradyzoite samples across genotypes (Fig. 3A). Of note, contrary to previous reports that *AAH1* is constitutive but *AAH2* is bradyzoite specific (20), the expression of both *AAH1* and *AAH2* appeared to go up in bradyzoites (Fig. 3A). As expected, the transcript for *AAH2* was absent from the knockout but restored in the complement (Fig. 3A). However, absolute expression of these genes remained very low; thus, relative fold change was not indicative of strong expression in the bradyzoite stage. This finding is consistent with data found in ToxoxDB. Based on microarray data for the type II ME49 strain (33), the expression levels of *AAH1* and *AAH2* are in the 15th and

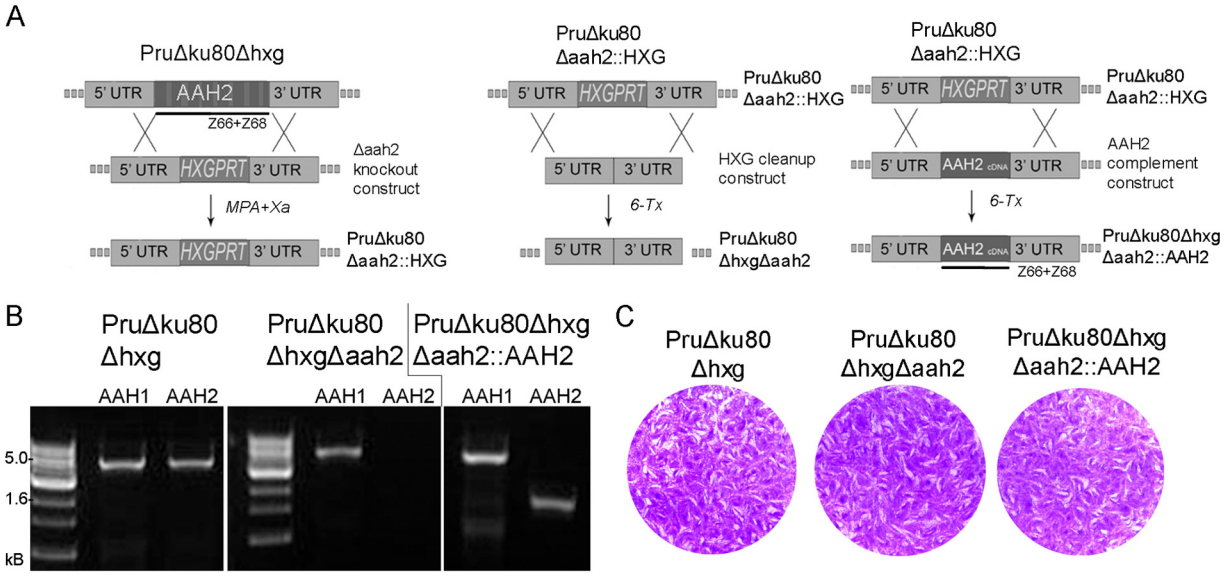

FIG 1 Generation of an *AAH2*-deficient strain and genetic complementation. (A) Schematic of *AAH2* knockout strategy. (Left) *HXGPRT* construct flanked by 5′ and 3′ regions from the *AAH2* genomic locus was used to knock out the *AAH2* gene in the PruΔ*ku80*Δ*hxg* background by double homologous crossover. MPA, mycophenolic acid; Xa, xanthine, which was used for selection. (Center) The deletion strain (Δ*aah2*::*HXG*) was transfected with cleanup construct to remove the *HXGPRT* drug marker. (Right) The deletion strain (Δ*aah2*::*HXG*) was complemented by replacing *HXGPRT* with a cDNA copy of *AAH2*. (B) Diagnostic PCR of the wild-type (PruΔ*ku80*Δ*hxg*), deletion mutant (PruΔ*ku80*Δ*hxg*Δ*aah2*), and complement (PruΔ*ku80*Δ*hxg*Δ*aah2*::*AAH2*) lines. Arrows show the respective primers used to confirm the genetic architecture (see Table S1 in the supplemental material). Expected product sizes were the following: *AAH1*, 4.820 kb; *AAH2*, 4.820 kb; *AAH2* cDNA, 1.698 kb. (C) Plaque assay measuring *in vitro* growth of strains on HFF monolayers stained with crystal violet.

30th percentiles among all *T. gondii* genes in tachyzoites and go up to the 35th and 40th percentiles, respectively, in bradyzoites. As a comparison, *BAG1*, a bradyzoite-specific protein that is induced in bradyzoites (34), has an expression level in the 60th percentile in tachyzoites, going up to the 100th percentile in bradyzoites.

Expression of *AAH1* and *AAH2* is very low in tachyzoites or bradyzoites. We sought to identify the localization of the parasite hydroxylases using both immunofluorescence and Western blot analysis. Using a double homologous recombination strategy with HXG selection as previously described, *AAH1* and *AAH2* were separately tagged with a Ty epitope (24), and parasites were screened for expression. Western blot analysis failed to identify detectable levels of either protein in bradyzoites (Fig. 3B). In tachyzoites (not shown) and in bradyzoites, no signal was visible for either Ty-tagged AAH protein by immunofluorescence (Fig. 3C). To differentiate between an absent signal due to minimal/low expression levels from an artifact of protein folding, another parasite line was created in which the *BAG1* promoter was used to overexpress Ty-tagged AAH2 (see Fig. S5 in the supplemental material). The resulting parasite line showed a clear Ty epitope signal by Western blotting (Fig. 3B) and immunofluorescence (Fig. 3C) when grown under bradyzoite-inducing conditions. However, we were unable to demonstrate cross-reactivity with the mammalian tyrosine hydroxylase antibody previously reported in the literature (15), even in the AAH2-overexpressing line (see Fig. S6). We also were unable to detect dopamine in PC12 cells using a previously reported technique (15 and data not shown). Taken together, these results suggest that our inability to detect proteins derived from *AAH1* and *AAH2* under native conditions is due to low levels of expression in both tachyzoites and bradyzoites.

Infection with *T. gondii* does not affect host dopamine levels *in vitro*. We investigated the effect of *T. gondii* infection on *in vitro* dopaminergic PC12 cell cultures *in vitro* and found that infection with tachyzoites did not significantly alter dopamine content (Fig. 4A and Table 1). To test for a dopaminergic effect in the bradyzoite stage, we stressed infected cells by raising the pH to 8.1, a treatment known to induce differentiation (31). Immunofluorescence analysis confirmed the presence of bradyzoite vacuoles within PC12 cells (see Fig. S7 in the supplemental material). Although we observed a 10-fold decrease in dopamine content per cell under the high-pH stress conditions, no difference in dopamine content was observed between infected and uninfected cells (Fig. 4B). In tachyzoite and bradyzoite cultures, neither deletion of *AAH2* nor bradyzoite-specific overexpression of *AAH2* resulted in significant differences in dopamine content. To rule out the possibility that increases in dopamine content were masked by the high endogenous dopamine stores of PC12 cells, which can reach up to 20 ng/10^5 cells, we repeated the experiment with SH-SY5Y cells that produce but do not store dopamine and again observed no increase in dopamine levels (data not shown).

Infection with *T. gondii* does not affect global or regional host dopamine levels *in vivo*. We initially tested for changes in the ability to form cysts in host brains *in vivo*. One thousand tachyzoites of each strain were injected i.p. into 6- to 8-week-old CD1 female mice, and brains were assayed 1 month postinfection for cyst formation. Both mutant and complement strains showed normal parasite cyst burden relative to that of wild-type parasites (Fig. 5A). Additionally, there was no difference in average cyst size between wild-type and Δ*aah2* knockout parasites (see Fig. S8 in the supplemental material). We also tested the ability of these cysts to survive digestion to induce oral transmission of infection. Five cysts were fed by oral gavage to naive 6- to 8-week-old CD1 mice, and serum was collected 1 month postinfection to assay infectivity by ELISA. All strains caused seroconversion in mice upon

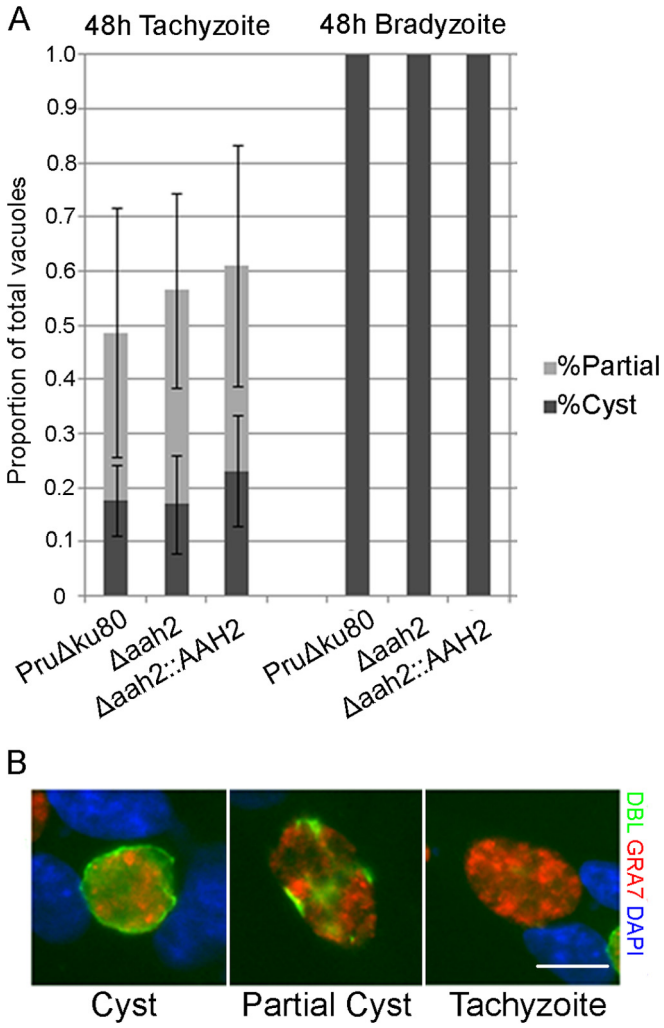

FIG 2 Differentiation into bradyzoites *in vitro*. (A) Formation of cysts by wild-type, Δ*aah2*, and Δ*aah2*::*AAH2* parasites in tachyzoite and bradyzoite conditions *in vitro*. Partial and fully formed cysts were enumerated based on staining with DBL. There was no significant difference in cyst formation in bradyzoite-induced parasites ($P = 1.00$) and no significant difference in cyst formation ($P = 0.66$) or partial cyst formation ($P = 0.88$) in tachyzoite conditions (both determined by one-way ANOVA; $n = 3$ experiments). (B) Representative pictures of intact, partial, and absent cyst formation in parasite vacuoles. Blue, 4′,6-diamidino-2-phenylindole (DAPI); red, GRA7; green, DBL. Scale bar, 10 μm.

feeding, indicating they are capable of normal oral transmission (see Fig. S9).

We observed no significant difference in whole-brain dopamine levels between mice infected with wild-type, Δ*aah2*, or Δ*aah2*::*AAH2* parasites compared to PBS controls (Fig. 5B). However, because the overall cyst burden was relatively low, ~100 cysts per brain, we repeated whole-brain dopamine assays with the more cyst-competent ME49 strain. At 1 month postinfection, cyst burden in ME49-infected mice was significantly higher (Fig. 5A), but brain dopamine levels were 20% lower than those of uninfected mice (Fig. 5B). This likely was due to persistent acute infection, as concurrent illness also was observed. Consequently, infection with ME49 parasites was repeated at a lower dose (200 tachyzoites), and brain dopamine was assayed 2 months postinfection, after acute illness was no longer visible. Despite slightly increased cyst burdens relative to those of Pru infection, brain dopamine levels still were not significantly different from those for uninfected mice (Fig. 5B). Overall there was no correlation relationship between cyst density and whole-brain dopamine for ME49-infected mice (Fig. 5C). We further investigated the possibility of changes in dopamine at the regional level, examining the striatum of infected and uninfected mice, and again we found no difference in dopamine levels between control and infected mice (see Fig. S10 in the supplemental material).

Finally, because all of the previous experiments were done with type II strains, we repeated the experiment using the type III C56 strain, reported previously (17). Five mice were infected i.p. with our standard dose (10^3 tachyzoites) and five mice with the dose used by Stibbs (10^4 tachyzoites) (17). Using either method, the brain cyst density was significantly lower at 1 month postinfection than that with the type II Pru or ME49 strains (e.g., 2/5 mice infected with 10^3 parasites and 3/5 mice infected with 10^4 parasites showed brain cyst densities below the detection limit of 20 cysts per brain [Fig. 5A]). Brain dopamine levels were not significantly different from those of uninfected mice at either dose (10^3 tachyzoites, $P = 0.13$; 10^4 tachyzoites, $P = 0.20$; Mann-Whitney test) (Fig. 5B).

DISCUSSION

Although *T. gondii*'s ability to manipulate rodent behavioral responses to the cat is well documented (5–13) and several studies suggest that the parasite manipulates dopamine signaling in the host brain (15, 17, 19, 20, 35), no parasite effectors have been found for these host alterations. We sought to test the hypothesis that the parasite genes *AAH1* and/or *AAH2*, which encode the catecholamine biosynthetic enzyme tyrosine hydroxylase, were responsible for the alterations of host dopamine levels observed *in vitro* (15) and *in vivo* (17). However, we were unable to demonstrate *T. gondii* infection having any effect on dopamine levels in the catecholaminergic cell line PC12 or in infected mouse brains. Furthermore, contrary to previous reports that described tyrosine hydroxylase within parasite bradyzoite cysts (15), we observed that levels of both *AAH1* and *AAH2* were extremely low and undetectable at native expression levels in both tachyzoites and bradyzoites, consistent with low expression levels observed in microarray data (previously reported in ToxoDB). Collectively, these studies indicate that *AAH* genes do not lead to global changes in dopamine production in the host, although they may contribute to local differences. Additionally, our findings suggest that *AAH* genes are involved in a different function, since *AAH1* is essential for growth in nondopaminergic cells.

We did not observe changes in global brain dopamine levels with either the Pru strain or the C56 strain, unlike what was previously reported (17). However, closer examination of this original study indicates that the significant difference reported can be attributed to very low variance in the sample rather than dramatic differences in the average values (17). Brain dopamine values in our sample values approximate those reported previously yet show higher variance, consistent with the expectation for animal studies. Our results are consistent with other reports that investigated dopamine and neurotransmitter levels in infected rodents. For example, Goodwin et al. (36) described minimal changes observed in dopamine, norepinephrine, and serotonin concentrations in the frontal cortex and striatum of chronically infected

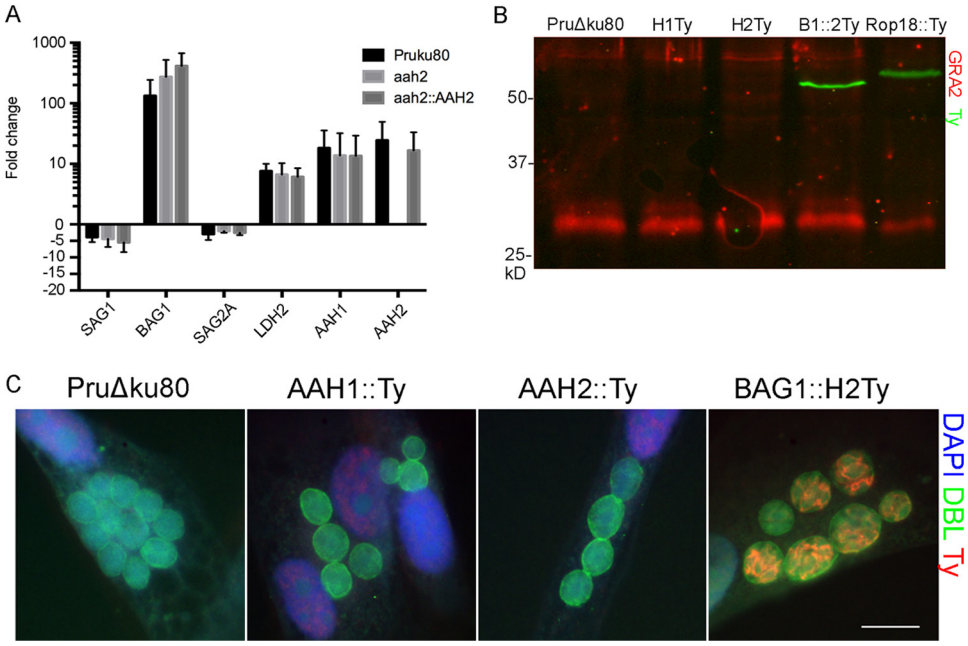

FIG 3 Differentiation and expression levels in tachyzoites and bradyzoites. (A) Quantitative real-time PCR comparing gene expression of bradyzoites relative to that of tachyzoites of wild-type, knockout (Δ*aah2*), and complemented (Δ*aah2*::*AAH2*) parasites. Stage-specific markers *SAG1*, *BAG1*, *SAG2A*, and *LDH2*, along with *AAH1* and *AAH2*, were monitored with gene-specific primers (see Table S1 in the supplemental material). Results are means ± standard deviations (SD) ($n = 3$ experiments). Excluding the expected differences in *AAH2* expression, expression differences between the genes probed were not significant ($P = 0.19$ by two-way ANOVA). (B) Western blot of bradyzoites expressing a Ty epitope-tagged AAH1 or AAH2 or a tagged copy of AAH2 driven by the BAG1 promoter. Red, GRA2; green, Ty. Expected protein sizes: AAH1 and AAH2, 55 kDa; GRA2 (dense granule protein 2), 28 kDa. (C) Immunofluorescent assay of AAH1-Ty-, AAH2-Ty-, and BAG1::H2Ty-tagged parasites differentiated into bradyzoites. Blue, DAPI; green, DBL; red, Ty. Scale bar, 10 μm.

mice. Similarly, Gatkowska et al. (37) noted profound changes in the ratios of dopamine, serotonin, and norepinephrine to their metabolites during acute infection, but which returned to baseline upon the establishment of chronic infection. Additionally, we did not observe differences in dopamine or related metabolite levels in the striatum, a region of the brain rich in dopaminergic terminals. It was recently suggested that expression of AAH enzymes in bradyzoites (detected with a commercial anti-tyrosine hydroxylase [TH] antibody) leads to elevated dopamine surrounding tissue cysts *in vivo* (15). We were unable to replicate these findings here, as the commercial antibody to TH did not react to *T. gondii* in our hands, even in the strain that overexpressed AAH2. Additionally, attempts to localize dopamine in PC12 cells were not successful, presumably because this small metabolite rapidly diffuses in fixed cells and tissues. Despite not observing global or regional changes, our experiments cannot rule out an effect of AAH enzymes on localized or transient dopamine levels in the host, which could in turn affect behavior. Further experiments using microdialysis monitoring may reveal highly localized changes to dopamine in the CNS and may be useful in studying the role of parasite infection and AAH enzymes on host signaling pathways.

Previous studies have indicated that infection with *T. gondii*

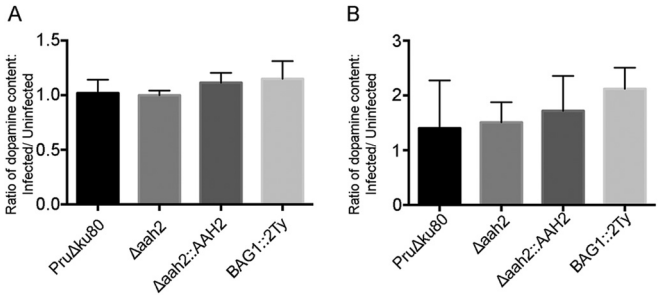

FIG 4 Production of dopamine in infected PC12 cells. (A) Comparison of infection with wild-type, knockout (Δ*aah2*), complement (Δ*aah2*::*AAH2*), or BAG1-2Ty overexpressor tachyzoites in PC12 cells ($P = 0.40$ by one-way ANOVA). Results are means ± SD ($n = 2$ to 5 replicates). The *y* axis shows the ratio of dopamine content per PC12 cell relative to uninfected PC12s. (B) Comparison of dopamine content in PC12 cells grown under bradyzoite conditions ($P = 0.4239$ by one-way ANOVA). Results are means ± SD ($n = 2$ to 4).

TABLE 1 Dopamine and metabolite content determined by HPLC[c]

Stage and strain	Dopac[a]	Dopamine	HVA[b]
Tachyzoite			
PruΔ*ku80*Δ*hxg*	0.84 ± 0.71	20.43 ± 1.95	2.71 ± 0.35
Δ*aah2*	0.60 ± 0.51	16.84 ± 2.25	2.42 ± 0.20
Δ*aah2*::*AAH2*	0.65 ± 0.63	18.38 ± 3.90	2.28 ± 0.86
Uninfected	0.25 ± 0.37	17.48 ± 5.68	1.99 ± 0.56
Bradyzoite			
PruΔ*ku80*Δ*hxg*	0.02 ± 0.03	0.96 ± 0.21	1.38 ± 0.10
Δ*aah2*	0.07 ± 0.01	1.37 ± 0.78	2.55 ± 0.31
Δ*aah2*::*AAH2*	0.25 ± 0.19	1.54 ± 0.12	1.88 ± 0.17
Uninfected	0.01 ± 0.01	0.71 ± 0.00	1.09 ± 0.82

[a] 3,4-Dihydroxyphenylacetic acid.
[b] Homovanillic acid.
[c] Results are reported as ng catecholamine/10^5 cells. Means ± standard deviations are shown from 3 technical replicates each (tachyzoites) and 2 each (bradyzoites) for one representative experiment.

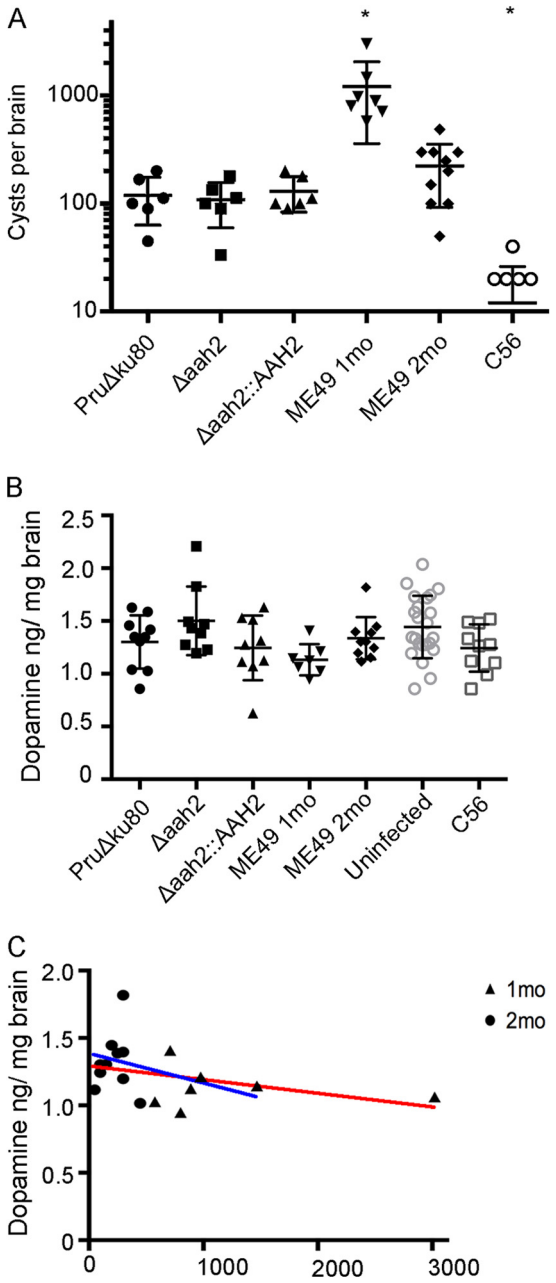

FIG 5 Dopamine content in the brain of control and infected mice. (A) Parasite cyst burden in whole brains of CD1 mice examined at 1 (1 mo) or 2 months (2 mo) postinfection. Infection with ME49 at 1 mo showed significantly higher cyst burden ($P = 0.0003$ by Kruskal-Wallis test with Dunn's multiple comparisons for Pru strains and ME49). Infection with the type III C56 strain showed significantly lower cyst burden ($P = 0.0003$ by Kruskal-Wallis test with Dunn's multiple comparisons for Pru strains and C56), with 5 of 10 mice showing cyst burdens below the detectable limit of 20 cysts/brain (not plotted). (B) Dopamine levels in total brain homogenates in uninfected and infected mice at 1 (1mo) or 2 (2mo) months postinfection. Dopamine levels were not significantly different between infected or uninfected animals or between infection strains ($P = 0.075$ by Kruskal-Wallis test with Dunn's multiple comparisons test). (C) Linear regression analysis between cyst density and brain dopamine concentration in mice infected with ME49 for 1 month (1mo) or 2 months (2mo). $R^2 = 0.1333$ (red). If the highest point in the linear regression was removed, $R^2 = 0.1175$ (blue).

increases dopamine production in PC12 cells (15) and implied that the *AAH1* and *AAH2* genes contribute to this by producing the precursor L-Dopa (20). However, we failed to reproduce the finding that infection elevates dopamine production in PC12 and also did not observe any change in SH-SY5Y cells when infected with either tachyzoites or bradyzoites. Given this finding, it was not surprising that no further changes were observed in dopamine production in these cell lines using mutants that lack *AAH2*. Based on immunofluorescence staining, qPCR, and microarray data, it also does not appear that *AAH* genes are highly expressed in bradyzoites. Finally, we did not observe increased levels of host dopamine production using a strain of *T. gondii* that overexpresses *AAH2*. This overexpressing strain was useful for demonstrating that *AAH2* appears to be secreted from bradyzoites and is detectable in the cyst matrix, as previously described (15). However, under native conditions it appears to be expressed at very low levels.

Collectively, our findings fail to support the original hypothesis that *T. gondii* AAH enzymes lead to globally elevated dopamine levels in the host. Instead, it is plausible that *AAH* genes are involved in other metabolic functions in the parasite. This possibility is supported by the fact that *AHH1* appears to be essential in nondopaminergic cells. Not only did repeated attempts to knock out this gene by double homologous cross over fail but we also have been unable to disrupt this gene using the much more efficient CRISPR system, which was recently described for *T. gondii* (38). The function of *AAH1* might be revealed using recently described strategies for inducible knockdown (39). Possible alternative activities of the hydroxylases include the production of dityrosine, which has previously been described in the oocyst walls of *Eimeria* (40, 41). Microarray data describe the upregulation of *AAH* genes in the oocyst stages of *T. gondii* (42), suggesting they participate in this process. However, such a role is unlikely to explain the essentiality of AAH1 in tachyzoites. Alternatively, because tetrahydrobiopterin likely is consumed as a cofactor by these hydroxylases, the *AAH* genes may serve as a sink for the output of the pterin pathway, which has been partially characterized in previous studies (43). Finally, although *T. gondii* is not known to produce melanin, which plays an important role in fungal virulence (44), the AAH enzymes could provide precursors to other catechol metabolites that are important in growth and/or virulence of *T. gondii*.

Although we did not find evidence for global changes in dopamine levels, infection by the parasite causes a number of global changes in the rodent brain. For example, infection causes low-level inflammation throughout the brain (45), affects the activity level of infected neurons (46), alters microRNA expression in cells (35), and causes changes in host gene expression in the frontal cortex of mice (12). Since chronic infection leads to activated microglia around many, but not all, tissue cysts (47), a potential cause of signaling and behavioral abnormalities would be inflammation. Interestingly, it was discovered that mice infected by attenuated parasites incapable of persisting as cysts in the brain still exhibited attraction to cat odor months after acute infection had been completely cleared and parasites were no longer detectable in the brain by PCR (13). These findings suggest that alteration or rewiring of the mouse brain during acute infection leads to alterations in rodent behavior. Such interactions are likely to be complex and will require extensive further study to uncover the basis for altered behavior in chronically infected animals.

ACKNOWLEDGMENTS

We are grateful to Jennifer Barks and Qiuling Wang for technical assistance and Stephen Beverley, Tim Holy, Beau Ances, Robert Yolken, and Mikhail Pletnikov for helpful advice.

This work was supported in part by a grant from the NIH (AI059176).

REFERENCES

1. **Dubey JP.** 2007. The history and life cycle of *Toxoplasma gondii*, p 1–17. *In* Weiss LM, Kim K (ed), *Toxoplasma gondii* the model Apicomplexan: perspectives and methods. Academic Press, Elsevier, New York, NY.
2. **Frenkel JK, Dubey JP, Miller NL.** 1970. *Toxoplasma gondii* in cats: fecal stages identified as coccidian oocysts. Science **167:**893–896. http://dx.doi.org/10.1126/science.167.3919.893.
3. **Dubey JP, Thulliez P.** 1993. Persistence of tissue cysts in edible tissues of cattle fed *Toxoplasma gondii* oocysts. Am J Vet Res **54:**270–273.
4. **Dubey JP, Dubey JP.** 2010. Toxoplasmosis of animals and humans, 2nd ed. CRC Press, Boca Raton, FL.
5. **Kaushik M, Knowles SC, Webster JP.** 2014. What makes a feline fatal in Toxoplasma gondii's fatal feline attraction? Infected rats choose wild cats. Integr Comp Biol **54:**118–128. http://dx.doi.org/10.1093/icb/icu060.
6. **Kaushik M, Lamberton PH, Webster JP.** 2012. The role of parasites and pathogens in influencing generalised anxiety and predation-related fear in the mammalian central nervous system. Hormones Behav **62:**191–201. http://dx.doi.org/10.1016/j.yhbeh.2012.04.002.
7. **Lamberton PH, Donnelly CA, Webster JP.** 2008. Specificity of the Toxoplasma gondii-altered behaviour to definitive versus non-definitive host predation risk. Parasitology **135:**1143–1150. http://dx.doi.org/10.1017/S0031182008004666.
8. **Vyas A, Kim KS, Giacomini N, Boothroyd JC, Sapolsky RM.** 2007. Behavioral changes induced by Toxoplasma infection of rodents are highly specific to aversion of cat odors. Proc Natl Acad Sci U S A **104:**6442–6447. http://dx.doi.org/10.1073/pnas.0608310104.
9. **Berdoy M, Webster JP, Macdonald DW.** 2000. Fatal attraction in rats infected with *Toxoplasma gondii*. Proc R Soc Lond B Biol Sci **267:**1591–1594. http://dx.doi.org/10.1098/rspb.2000.1182.
10. **Kannan G, Moldovan K, Xiao JC, Yolken RH, Jones-Brando L, Pletnikov MV.** 2010. Toxoplasma gondii strain-dependent effects on mouse behaviour. Folia Parasitol **57:**151–155. http://dx.doi.org/10.14411/fp.2010.019.
11. **Golcu D, Gebre RZ, Sapolsky RM.** 2014. Toxoplasma gondii influences aversive behaviors of female rats in an estrus cycle dependent manner. Physiol Behav **135:**98–103. http://dx.doi.org/10.1016/j.physbeh.2014.05.036.
12. **Xiao J, Kannan G, Jones-Brando L, Brannock C, Krasnova IN, Cadet JL, Pletnikov M, Yolken RH.** 2012. Sex-specific changes in gene expression and behavior induced by chronic Toxoplasma infection in mice. Neuroscience **206:**39–48. http://dx.doi.org/10.1016/j.neuroscience.2011.12.051.
13. **Ingram WM, Goodrich LM, Robey EA, Eisen MB.** 2013. Mice infected with low-virulence strains of Toxoplasma gondii lose their innate aversion to cat urine, even after extensive parasite clearance. PLoS One **8:**e75246. http://dx.doi.org/10.1371/journal.pone.0075246.
14. **Webster JP, McConkey GA.** 2010. Toxoplasma gondii-altered host behaviour: clues as to mechanism of action. Folia Parasitol **57:**95–104. http://dx.doi.org/10.14411/fp.2010.012.
15. **Prandovszky E, Gaskell E, Martin H, Dubey JP, Webster JP, McConkey GA.** 2011. The neurotropic parasite Toxoplasma gondii increases dopamine metabolism. PLoS One **6:**e23866. http://dx.doi.org/10.1371/journal.pone.0023866.
16. **Skallova A, Kodym P, Frynta D, Flegr J.** 2006. The role of dopamine in Toxoplasma-induced behavioural alterations in mice: an ethological and ethopharmacological study. Parasitology **133:**525–535. http://dx.doi.org/10.1017/S0031182006000886.
17. **Stibbs HH.** 1985. Changes in brain concentrations of catecholamines and indoleamines in Toxoplasma gondii infected mice. Ann Trop Med Parasitol **79:**153–157.
18. **Jones-Brando L, Torrey EF, Yolken R.** 2003. Drugs used in the treatment of schizophrenia and bipolar disorder inhibit the replication of Toxoplasma gondii. Schizophr Res **62:**237–244. http://dx.doi.org/10.1016/S0920-9964(02)00357-2.
19. **Webster JP, Lamberton PH, Donnelly CA, Torrey EF.** 2006. Parasites as causative agents of human affective disorders? The impact of anti-psychotic, mood-stabilizer and anti-parasite medication on Toxoplasma gondii's ability to alter host behaviour. Proc Biol Sci **273:**1023–1030. http://dx.doi.org/10.1098/rspb.2005.3413.
20. **Gaskell EA, Smith JE, Pinney JW, Westhead DR, McConkey GA.** 2009. A unique dual activity amino acid hydroxylase in Toxoplasma gondii. PLoS One **4:**e4801. http://dx.doi.org/10.1371/journal.pone.0004801.
21. **Fox BA, Falla A, Rommereim LM, Tomita T, Gigley JP, Mercier C, Cesbron-Delauw MF, Weiss LM, Bzik DJ.** 2011. Type II Toxoplasma gondii KU80 knockout strains enable functional analysis of genes required for cyst development and latent infection. Eukaryot Cell **10:**1193–1206. http://dx.doi.org/10.1128/EC.00297-10.
22. **Lunde MN, Jacobs L.** 1964. Properties of Toxoplasma Lysates Toxic to Rabbits on Intravenous Injection. J Parasitol **50:**49–51.
23. **Sibley LD, Boothroyd JC.** 1992. Virulent strains of *Toxoplasma gondii* comprise a single clonal lineage. Nature **359:**82–85.
24. **Bastin P, Bagherzadeh Z, Matthews KR, Gull K.** 1996. A novel epitope tag system to study protein targeting and organelle biogenesis in *Trypanosoma brucei*. Mol Biochem Parasitol **77:**235–239.
25. **Donald RGK, Roos DS.** 1998. Gene knock-outs and allelic replacements in *Toxoplasma gondii*: HXGPRT as a selectable marker for hit-and-run mutagenesis. Mol Biochem Parasitol **91:**295–305.
26. **Pfefferkorn ER, Bzik DJ, Honsinger CP.** 2001. Toxoplasma gondii: mechanism of the parasitostatic action of 6-thioxanthine. Exp Parasitol **99:**235–243. http://dx.doi.org/10.1006/expr.2001.4673.
27. **Fux B, Nawas J, Khan A, Gill DB, Su C, Sibley LD.** 2007. *Toxoplasma gondii* strains defective in oral transmission are also defective in developmental stage differentiation. Infect Immun **75:**2580–2590. http://dx.doi.org/10.1128/IAI.00085-07.
28. **Livak KJ, Schmittgen TD.** 2001. Analysis of relative gene expression data using real-time quantitative PCR and the 2(-delta-delta C(T)) method. Methods **25:**402–408. http://dx.doi.org/10.1006/meth.2001.1262.
29. **Shen B, Sibley LD.** 2014. Toxoplasma aldolase is required for metabolism but dispensable for host-cell invasion. Proc Natl Acad Sci U S A **111:**3567–3572. http://dx.doi.org/10.1073/pnas.1315156111.
30. **Lotharius J, O'Malley KL.** 2000. The parkinsonism-inducing drug 1-methyl-4-phenylpyridinium triggers intracellular dopamine oxidation. A novel mechanism of toxicity. J Biol Chem **275:**38581–38588. http://dx.doi.org/10.1074/jbc.M005385200.
31. **Soête M, Camus D, Dubremetz JF.** 1994. Experimental induction of bradyzoite-specific antigen expression and cyst formation by the RH strain of *Toxoplasma gondii in vitro*. Exp Parasitol **78:**361–370.
32. **Boothroyd JC, Black M, Bonnifoy S, Hehl A, Knoll L, Manger ID, Ortega-Barria E, Tomavo S.** 1997. Genetic and biochemical analysis of development in *Toxoplasma gondii*. Philos Trans R Soc Lond **352:**1347–1354.
33. **Behnke M, Wooten JC, Lehmann M, Radke J, Lucas O, Nawas J, Sibley LD, White M.** 2010. Coordinated progression through two subtranscriptions underlies the tachyzoite cycle of Toxoplasma gondii. PLoS One **5:**e12354. http://dx.doi.org/10.1371/journal.pone.0012354.
34. **Bohne W, Gross U, Ferguson DJP, Hessemann J.** 1995. Cloning and characterization of a bradyzoite-specifically expressed gene (*hsp30/bag1*) of *Toxoplasma gondii*, related to genes encoding small heat-shock proteins of plants. Mol Microbiol **16:**1221–1230.
35. **Xiao J, Li Y, Prandovszky E, Karuppagounder SS, Talbot CC, Jr, Dawson VL, Dawson TM, Yolken RH.** 2014. MicroRNA-132 dysregulation in Toxoplasma gondii infection has implications for dopamine signaling pathway. Neuroscience **268:**128–138. http://dx.doi.org/10.1016/j.neuroscience.2014.03.015.
36. **Goodwin D, Hrubec TC, Klein BG, Strobl JS, Werre SR, Han Q, Zajac AM, Lindsay DS.** 2012. Congenital infection of mice with Toxoplasma gondii induces minimal change in behavior and no change in neurotransmitter concentrations. J Parasitol **98:**706–712. http://dx.doi.org/10.1645/GE-3068.1.
37. **Gatkowska J, Wieczorek M, Dziadek B, Dzitko K, Dlugonska H.** 2013. Sex-dependent neurotransmitter level changes in brains of Toxoplasma gondii infected mice. Exp Parasitol **133:**1–7. http://dx.doi.org/10.1016/j.exppara.2012.10.005.
38. **Shen B, Brown KM, Lee TD, Sibley LD.** 2014. Efficient gene disruption in diverse strains of *Toxoplasma gondii* using CRISPR/CAS9. mBio **5:**e01114–14. http://dx.doi.org/10.1128/mBio.01114-14.
39. **Andenmatten N, Egarter S, Jackson AJ, Jullien N, Herman JP, Meissner M.** 2012. Conditional genome engineering in *Toxoplasma gondii* uncovers

alternative invasion mechanisms. Nat Methods **10:**125–127. http://dx.doi.org/10.1038/nmeth.2301.

40. **Belli SI, Wallach MG, Luxford C, Davies MJ, Smith NC.** 2003. Roles of tyrosine-rich precursor glycoproteins and dityrosine- and 3,4-dihydroxyphenylalanine-mediated protein cross-linking in development of the oocyst wall in the coccidian parasite Eimeria maxima. Eukaryot Cell **2:**456–464. http://dx.doi.org/10.1128/EC.2.3.456-464.2003.
41. **Belli SI, Wallach MG, Smith NC.** 2003. Cloning and characterization of the 82 kDa tyrosine-rich sexual stage glycoprotein, GAM82, and its role in oocyst wall formation in the apicomplexan parasite, Eimeria maxima. Gene **307:**201–212. http://dx.doi.org/10.1016/S0378-1119(03)00451-7.
42. **Fritz HM, Buchholz KR, Chen X, Durbin-Johnson B, Rocke DM, Conrad PA, Boothroyd JC.** 2012. Transcriptomic analysis of toxoplasma development reveals many novel functions and structures specific to sporozoites and oocysts. PLoS One **7:**e29998. http://dx.doi.org/10.1371/journal.pone.0029998.
43. **Wang Q, Hauser V, Read M, Wang P, Hanson AD, Sims PF, Hyde JE.** 2006. Functional identification of orthologous genes encoding pterin recycling activity in Plasmodium falciparum and Toxoplasma gondii. Mol Biochem Parasitol **146:**109–112. http://dx.doi.org/10.1016/j.molbiopara.2005.11.002.
44. **Revankar SG, Sutton DA.** 2010. Melanized fungi in human disease. Clin Microbiol Rev **23:**884–928. http://dx.doi.org/10.1128/CMR.00019-10.
45. **Munoz M, Liesenfeld O, Heimesaat MM.** 2011. Immunology of Toxoplasma gondii. Immunol Rev **240:**269–285. http://dx.doi.org/10.1111/j.1600-065X.2010.00992.x.
46. **Haroon F, Handel U, Angenstein F, Goldschmidt J, Kreutzmann P, Lison H, Fischer KD, Scheich H, Wetzel W, Schluter D, Budinger E.** 2012. Toxoplasma gondii actively inhibits neuronal function in chronically infected mice. PLoS One **7:**e35516. http://dx.doi.org/10.1371/journal.pone.0035516.
47. **Evans AK, Strassmann PS, Lee IP, Sapolsky RM.** 2014. Patterns of Toxoplasma gondii cyst distribution in the forebrain associate with individual variation in predator odor avoidance and anxiety-related behavior in male Long-Evans rats. Brain Behav Immun **37:**122–133. http://dx.doi.org/10.1016/j.bbi.2013.11.012.